

## 14. MAJOR-ELEMENT CHEMISTRY AND ALTERATION MINERALOGY OF VOLCANIC ASH, SITE 808 IN THE NANKAI TROUGH<sup>1</sup>

Harue Masuda,<sup>2</sup> Hiroaki Tanaka,<sup>2</sup> Toshitaka Gamo,<sup>3</sup> Wonn Soh,<sup>4</sup> and Asahiko Taira<sup>3</sup>

### ABSTRACT

Mineralogical and major-element compositions of 72 samples of volcanic ash, recovered from Site 808 at Nankai Trough during Leg 131, were analyzed in relation to the early diagenetic alteration. Alteration products are first observed at the following depths: smectite, 200 mbsf; clinoptilolite, 646 mbsf; and analcite, 810 mbsf.

Glass decomposition dominates over authigenic mineral formation between 200 and 550 mbsf in the sediment column, whereas mineral formation becomes dominant below 550 mbsf. Based on the X-ray diffraction patterns, a broad and asymmetric peak of 15Å suggests a presence of illite/smectite (I/S) mixed-layered minerals in a sample from 646 mbsf. I/S mixed-layered mineral formation, however, rarely occurs even at the bottom of the sediment column (1290 mbsf) at 120° C. This is possibly because zeolite (especially clinoptilolite) formed in the ash interferes with illite formation in the smectite.

The formation of alteration minerals affects the major-element chemistry of the ash and the interstitial waters. H<sub>4</sub>SiO<sub>4</sub> concentrations in interstitial waters increase during glass decomposition and decrease with smectite and clinoptilolite formation. K is removed from interstitial water into smectite and/or clinoptilolite. Mg is fixed into smectite (and/or chlorite).

### INTRODUCTION

The alteration of volcanic ash is considered to be an essential process in the diagenesis of marine sediments. For example, Weaver (1958) suggested that most of the expanded clays in marine sediments were derived from volcanic glass, and that potassium was fixed into expandable clays and later illite from the coexisting pore water. In several studies of chemical variations of interstitial water, previous workers have suggested that low-temperature alteration of ash affected interstitial water chemistry (e.g., Lawrence et al., 1979; Gieskes and Lawrence, 1981; Gieskes et al., 1990a, b). Matsuhisa and Matsumoto (1986) attributed the variation of δ<sup>18</sup>O and Mg content of interstitial waters recovered from the Nankai Trough during Leg 87 to ash alteration. From the onboard chemical analyses of interstitial waters retrieved from Site 808, Leg 131 (Fig. 1), Shipboard Scientific Party (1991) also pointed out that the chemical variations of interstitial water were partly affected by the alteration of ash.

In his report on the lithology and physical properties of sediments in subduction zones, Vrolijk (1990) discussed the importance of smectite-rich sediments. He suggested that smectite-rich strata derived from alteration of volcanic ash are structurally weak and that décollement zones may be preferentially formed in the smectite-rich layers.

The alteration of ash is also thought to be an important process in the geochemical cycle of oceanic sediments. However, little is known about the mineralogical and chemical variations of volcanic ash itself, because it is difficult to obtain a suite of pure volcanic ash samples from the same sediment column.

The continental slope of Nankai Trough (Fig. 1) is a well-documented modern accretionary prism in the Pacific Ocean. We selected 72 samples of volcanic ash from Site 808, where a complete sediment column was obtained from the ocean floor, through the décollement, to the underlying basalt. Because these samples originally have a high volcanic glass content, they provide a good opportunity for establishing a model of ash alteration at the early stage of diagenesis.

In this paper, we present the alteration mineralogy and major-element chemistry of the ash samples and discuss the effect of ash

alteration on the chemistry of interstitial fluids. The chemistry of bulk samples demonstrates that the decomposition of ash and the subsequent formation of authigenic smectite and zeolites play important roles in controlling interstitial water chemistry.

### SAMPLES

Site 808 is located at the toe of the Nankai accretionary prism. The sediments at Site 808 (0 to 1290 mbsf) can be broadly classified into two groups; clastic material transported by turbidity currents (dominating the upper portion of the sediment column above ca. 600 mbsf), and hemipelagic sediments deposited on the oceanic crust of Shikoku Basin in the lower portion (Shipboard Scientific Party, 1991). The facies association reported by the Shipboard Scientific Party, with location of 72 ash samples, is shown in Figure 2. The age of the basal sediment is between 13.6 and 15 Ma (Shipboard Scientific Party, 1991). Ash layers are especially concentrated in the interval from 557 to 824 mbsf. This interval corresponds to the trench-to-basin transition and the upper Shikoku Basin facies (Fig. 2A); the age of these sediments is between 0.28 and 2.65 Ma (Shipboard Scientific Party, 1991). The décollement zone extends from 945 to 965 mbsf in the lower Shikoku Basin facies. Only five samples of ash were recovered from this interval.

The 13 ash samples between 1245 and 1275 mbsf are apparently different from the ash above 1245 mbsf. These 13 ash samples are white and contain quartz grains about 1 mm diameter, based on optical observation. They were collected from various locations within the same ash layer of 45 m thickness. This ash layer was silicified and well consolidated, and the original glass is completely altered.

### ANALYTICAL METHOD

Mineralogical compositions were determined by X-ray diffraction using a Ni-target CuKα radiation at 30 kV and 10 mA. Randomly mounted air-dried bulk samples of ca. 200 mg were used for this purpose. For identification of illite/smectite mixed-layered minerals (I/S), glycolated samples were also scanned. The illite content in the I/S, however, was not determined in this study. The weight % of clay minerals was estimated from the peak height of the (001) reflection. Pure smectite diluted by powdered quartz glass was used for calibration. Reproducibility of clay contents for duplicated samples was within ±5%.

<sup>1</sup> Hill, I.A., Taira, A., Firth, J.V., et al., 1993. *Proc. ODP, Sci. Results*, 131: College Station, TX (Ocean Drilling Program).

<sup>2</sup> Department of Geosciences, Osaka City University, Sumiyoshi, Osaka 558, Japan.

<sup>3</sup> Ocean Research Institute, University of Tokyo, Nakano, Tokyo 164, Japan.

<sup>4</sup> Department of Earth Sciences, Shizuoka University, Otani, Shizuoka 422, Japan.

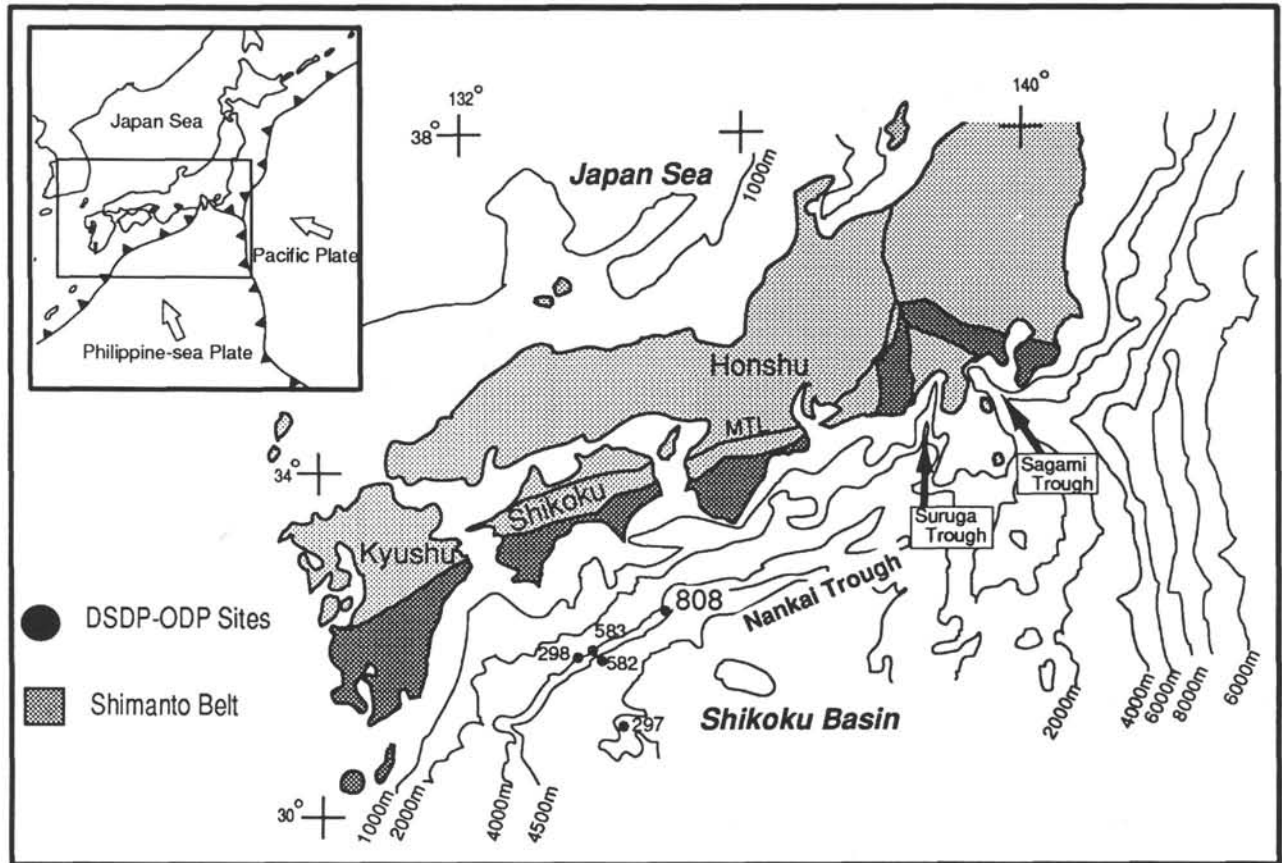


Figure 1. Location of Site 808, Leg 131.

For major chemical analyses, the samples were ultrasonically stirred with ultrafiltrated water to remove dissolved salts, and the residues were collected by centrifugation and sedimentation. This procedure was repeated at least four times and the ash was dried for 24 hr at 110° C. The dried samples were ignited at about 900° C for 1 hr. After ignition the ash samples are regarded as free from organic matter and volatile components such as carbonate and water. Lithium borate and a heat-treated, powdered sample (10:1) was fused in a 5% Au-containing platinum crucible for 8 min. at 1200° C to make a glass bead for quantitative analysis by X-ray fluorescence (XRF). The elemental analyses performed by XRF are Si, Al, Ti, Mg, Ca, Fe as Fe<sup>3+</sup>, Mn, Na, K, and P. All elemental compositions are expressed as weight % of the oxide form. Accuracy and reproducibility of measurement were checked by standard rock samples supplied by the Geological Survey of Japan. Measurement error of each element is within ±2%.

## RESULTS AND DISCUSSION

### Mineralogy

Minerals identified by the X-ray diffraction pattern of bulk ash layers are listed in Table 1. As noted before, the weight % of the constituent minerals except for total clay was not estimated. Thus, the mineral abundances are uncorrected intensities of characteristic peaks of each mineral.

Because the studied ash layers are ocean floor deposits derived from subaerial volcanism, the samples also contain detrital minerals. All ash samples contain quartz, feldspar, chlorite, and calcite. Most of the calcite must be originally of biogenic origin. The intensities of X-ray diffraction peaks of quartz, feldspar, and chlorite are slightly greater in the uppermost 556 mbsf of the sediment column, where

most sediments were affected by turbidity currents, in contrast to the lower portion, below 556 mbsf. Illite of 2M<sub>1</sub> polytype, indicating a detrital origin, is also a component of the uppermost 557 mbsf of sediment, though its concentration decreases with depth. Hornblende was frequently observed in the interval from 580 to 850 mbsf, which supports the possibility of a volcanic origin.

Figure 2B shows the alteration mineral assemblage of the ash layers. The relative concentrations of the alteration minerals estimated from X-ray diffraction data are plotted as a function of depth in Figures 2C–2E. The first downhole appearance of smectite recognized as the appearance of a 15-Å peak, was detected in the bulk sample from 200 mbsf. Below 557 mbsf, the concentration of clay minerals drastically increases with depth. A broad and asymmetric peak of the (001) clay mineral reflection suggests the occurrence of mixed-layered I/S in ash from 645 mbsf, where the temperature is about 60° C. From the on-board analysis, I/S formation was indicated by X-ray diffraction patterns of samples from the sediment column at ca. 530 mbsf (Shipboard Scientific Party, 1991). Underwood et al. (this volume) observed that I/S was detected in shales from 550 mbsf. They also reported that the illite composition in I/S increased with depth, with the illite content in I/S reaching almost 80% at the base of the sediment column at about 120° C. Both of the reported depths of I/S appearance are shallower than its possible appearance in ash. The X-ray diffraction peak of (001) clay mineral reflection in the ash samples becomes sharper and more symmetric with increasing depth, and illite formation in mixed-layered I/S does not occur even in the samples from the base of the sediment column, where smectite is still the most abundant phase of the authigenic clay minerals.

Mixed-layered I/S is widely recognized as a transition mineral phase in the transformation of smectite to illite during diagenesis (e.g., Weaver, 1958; Dunoyer de Segonzac, 1970). For the sedimen-

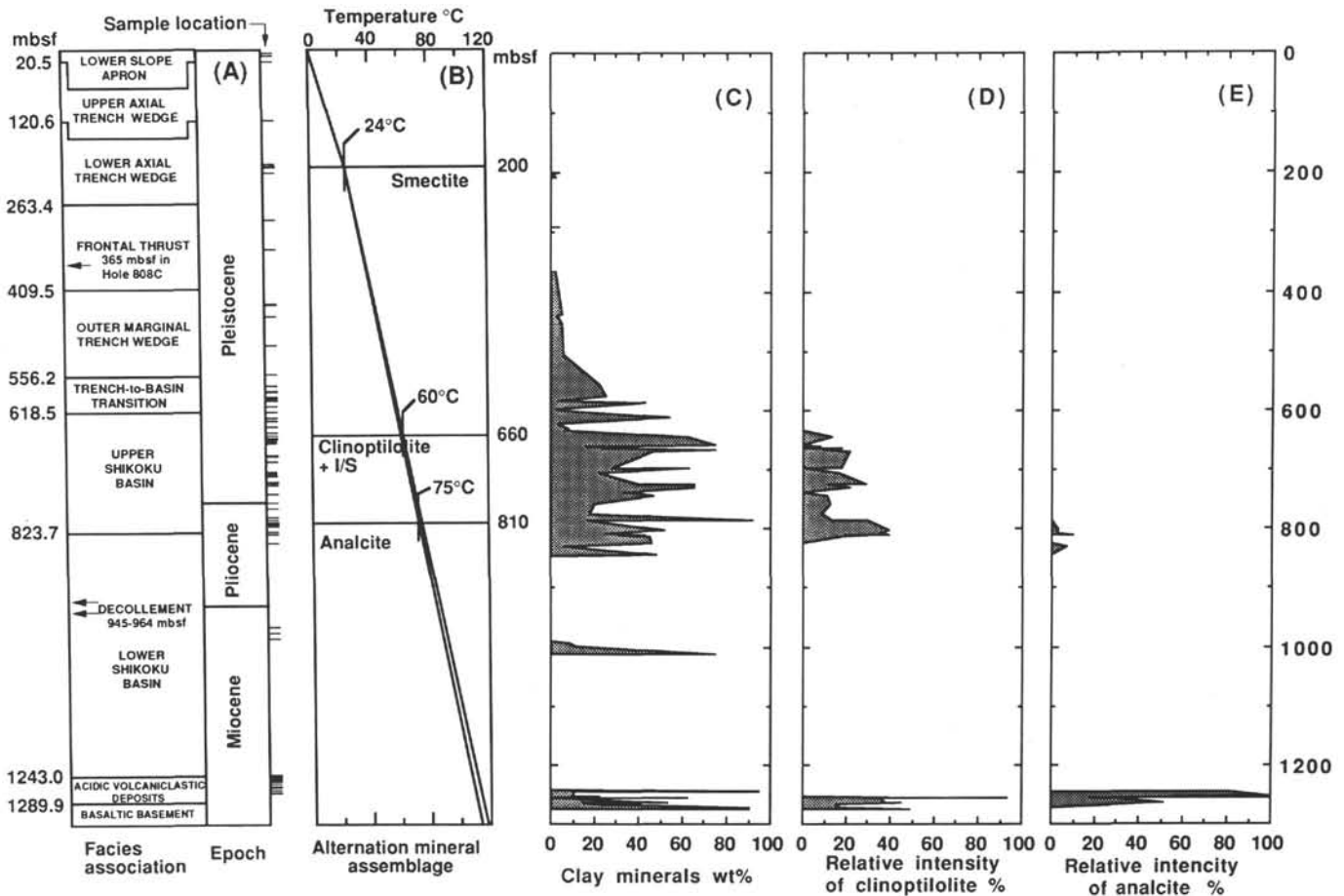


Figure 2. Facies association, alteration mineral assemblage of the sediment column, and occurrence of alteration minerals in layers of volcanic ash. Facies association (A) and temperature gradient (B) are from Taira, Hill, Firth, et al. (1991). Weight % of clay minerals (C) is calculated from X-ray diffraction intensities of (002) reflection. Relative intensities of clinoptilolite (D) and analcite (E) are expressed by the peak intensities (%) of the most intense peaks of X-ray diffraction.

tary basin along the coast of the Gulf of Mexico, Perry and Hower (1970) stated that the position of the smectite-to-illite transition zone is independent of geologic age and formation boundaries. They also determined that temperature is more important for the transition than pressure, and suggested that the transition starts at approximately 55° C. The appearance of mixed-layered I/S in Site 808 shales is in accordance with their observation. However, the incomplete formation of I/S in volcanic ash suggests that temperature is not the only control on I/S formation during diagenesis.

Tri-octahedral smectites are known to form in volcanic ash, with the tri-octahedral smectites being more stable than di-octahedral smectites at higher temperature (Anjos, 1986). This is not the case, however, because 1.5 Å of (006) reflection indicates that the clay mineral formed in the studied ash is di-octahedral.

In the sediment column studied, two zeolites were also observed as products of diagenesis. As shown in Figure 2D, clinoptilolite appears at about the same depth as possible mixed-layered I/S. Another zeolite, analcite, occurs below 810 mbsf where the temperature is greater than about 75° C (Fig. 2E). Altaner and Grim (1990) reported clinoptilolite and smectite formation during diagenetic alteration of vitric tuff in Miocene formation in eastern Oregon. They observed that the smectite coexisting with K-rich clinoptilolite is depleted in K. It is plausible that K-rich clinoptilolite formation interferes with the transformation of smectite to illite. Further information on I/S in volcanic ash and the chemical compositions of each separated mineral phase will be necessary to clarify the different formation mechanisms of I/S mixed-layered minerals between volcanic ash and shales.

### Major-Element Chemistry

The analytical data pertaining to the major chemical constituents of the bulk ash samples are given in Table 2, and some important constituents are plotted in Figure 3. The range of observed  $\text{TiO}_2/\text{Al}_2\text{O}_3$  ratios (0.01 to 0.05; Fig. 3B) is within the expected range for ash with an andesitic to rhyolitic composition derived from the Japanese Islands. For example, andesites from Sakurajima, one of the biggest and most active volcanos in Japan, have  $\text{TiO}_2/\text{Al}_2\text{O}_3$  ratios of 0.03 to 0.08 (Oba et al., 1980), while the ratio for pumice from Asama volcano is about 0.035 (Sato et al., 1989). Rhyolitic rocks have a smaller ratio than the andesites (e.g., 0.02 to 0.03 for volcanic glass tephros from Aso volcano; Machida and Momose, 1985). The apparent ratio of  $\text{TiO}_2/\text{Al}_2\text{O}_3$  of bulk ash may be higher than that of pure glass because of the contamination of basic minerals such as chlorite and amphiboles. The higher  $\text{TiO}_2/\text{Al}_2\text{O}_3$  ratio in the upper portion of the Site 808 sediment column as compared to the lower portion is concordant with the higher intensities of chlorites and amphiboles in the upper portion. If chemical analysis of pure glass were to be performed, the ash samples would become more rhyolitic than the present estimation.

Although decrease of the  $\text{TiO}_2/\text{Al}_2\text{O}_3$  ratio with depth indicates a more rhyolitic ash composition, the  $\text{SiO}_2/\text{Al}_2\text{O}_3$  ratio also generally decreases with increasing depth (Fig. 3). This is due to a higher solubility of Si relative to Al in the interstitial water.  $\text{SiO}_2$  is generally released to interstitial waters when volcanic glass decomposes, whereas Al and Ti tend to remain in the solid phase.

In Figure 4, the relation of  $\text{MgO}/\text{Al}_2\text{O}_3$  and  $\text{K}_2\text{O}/\text{Al}_2\text{O}_3$  to  $\text{SiO}_2/\text{Al}_2\text{O}_3$  are shown for ash from five depth intervals defined by the

**Table 1. Peak intensities by X-ray diffraction of minerals in volcanic ash from Site 808.**

Sample	mbsf	Qz	Feld	Ill	Chl	Cal	Ho	Clay	CP	Anal
131-808A-										
1H-1, 71-73 cm	3.7	100.0	77.8	15.3	22.8	0.0	0.0	0.0	0.0	0.0
2H-1, 77-79	7.1	100.0	56.5	31.5	39.7	62.5	0.0	0.0	0.0	0.0
3H-2, 41-43	17.6	100.0	91.0	21.7	25.9	12.7	0.0	0.0	0.0	0.0
131-808B-										
2X-1, 80-82 cm	121.4	100.0	38.1	4.2	5.7	20.9	0.0	0.0	0.0	0.0
9X-4, 92-94	193.6	100.0	50.8	10.0	15.2	35.1	0.0	0.0	0.0	0.0
10X-2, 142-144	200.3	100.0	49.2	6.6	11.1	24.9	0.0	2.8	0.0	0.0
10X-3, 52-54	200.9	37.8	31.8	0.0	0.0	0.0	0.0	0.0	0.0	0.0
11X-1, 115-117	208.0	100.0	72.9	60.8	81.8	31.5	0.0	0.0	0.0	0.0
20X-2, 32-33	289.7	100.0	80.7	63.1	51.1	0.0	0.0	2.8	0.0	0.0
131-808C-										
8R-1, 17-19 cm	366.1	100.0	38.6	5.7	9.4	22.5	0.0	0.0	0.0	0.0
15R-3, 62-63	437.3	100.0	56.4	11.0	16.0	0.0	0.0	4.3	0.0	0.0
15R-4, 33-34	438.5	100.0	65.3	36.5	38.3	0.0	0.0	1.8	0.0	0.0
17R-1, 73-75	453.4	79.6	33.7	7.2	8.8	64.1	0.0	3.9	0.0	0.0
22R-3, 122-124	505.2	100.0	42.6	12.2	14.9	18.6	0.0	4.8	0.0	0.0
27R-6, 32-33	557.1	0.0	96.8	0.0	0.0	31.7	0.0	21.5	0.0	0.0
29R-6, 38-39	575.0	0.0	100.0	0.0	0.0	19.1	0.0	25.1	0.0	0.0
30R-4, 99-100	583.8	54.6	35.4	3.1	0.0	27.2	0.0	3.1	0.0	0.0
30R-5, 119-120	585.5	100.0	88.0	0.0	4.0	20.6	51.4	47.4	0.0	0.0
32R-1, 128-130	598.6	46.9	50.0	0.0	2.6	0.0	0.0	3.1	0.0	0.0
32R-1, 142-144	598.7	38.0	42.6	7.7	7.2	0.0	0.0	4.1	0.0	0.0
32R-1, 147-149	598.8	97.4	8.2	0.0	0.0	0.0	0.0	2.1	0.0	0.0
32R-2, 82-84	599.6	31.8	63.6	0.0	0.0	0.0	4.6	3.0	0.0	0.0
33R-4, 4-6	611.4	28.7	42.4	0.0	0.0	0.0	7.8	62.1	0.0	0.0
34R-4, 126-128	622.3	69.5	31.2	8.1	7.1	100.0	0.0	2.0	0.0	0.0
35R-CC	630.0	71.4	28.9	0.0	3.2	17.3	0.0	6.8	0.0	0.0
35R-6, 60-62	634.3	62.3	27.2	0.0	3.7	20.4	0.0	6.3	0.0	0.0
37R-1, 30-32	645.8	100.0	96.9	0.0	0.0	0.0	0.0	65.4	13.0	0.0
38R-2, 67-68	657.1	100.0	42.9	0.0	0.0	24.2	0.0	80.8	0.0	0.0
38R-5, 83-85	661.7	64.7	52.9	12.8	18.7	0.0	0.0	15.0	8.0	0.0
38R-6, 69-71	663.1	0.0	99.1	0.0	0.0	0.0	0.0	40.2	0.0	0.0
38R-6, 76-78	663.2	23.9	66.3	0.0	0.0	0.0	0.0	27.2	0.0	0.0
39R-1, 47-49	665.0	100.0	43.1	9.0	6.9	45.7	0.0	22.3	18.1	0.0
39R-3, 31-33	667.8	33.1	100.0	0.0	0.0	0.0	0.0	90.6	10.0	0.0
39R-3, 52-54	668.0	42.1	37.6	0.0	0.0	23.0	0.0	55.2	21.8	0.0
42R-2, 90-92	695.9	100.0	63.0	6.9	11.0	43.9	0.0	36.4	17.9	0.0
42R-4, 15-17	698.2	44.6	38.6	0.0	0.0	0	0.0	72.8	0.0	0.0
43R-2, 115-117	705.9	100.0	80.7	34.6	11.0	0.0	0.0	21.9	16.1	0.0
45R-3, 7-9	725.1	50.3	100.0	0.0	5.1	20.2	46.1	43.8	28.7	0.0
45R-3, 35-37	725.6	35.8	63.7	0.0	0.0	24.6	0.0	54.8	14.5	0.0
45R-3, 61-63	725.6	0.0	100.0	0.0	0.0	19.8	37.5	65.1	12.0	0.0
45R-6, 26-28	729.8	72.2	31.6	0.0	0.0	19.3	0.0	73.7	21.6	0.0
46R-5, 126-129	739.0	47.8	91.8	0.0	0.0	17.6	5.5	31.3	0.0	0.0
46R-5, 135-137	739.1	49.5	78.8	0.0	0.0	19.6	8.2	38.6	0.0	0.0
47R-2, 114-116	743.8	100.0	67.4	0.0	0.0	14.0	35.5	52.3	11.1	0.0
48R-6, 139-140	758.5	100.0	77.9	14.7	14.2	19.6	0.0	20.2	12.5	0.0
50R-5, 2-4	775.6	100.0	62.6	4.8	5.9	36.4	0.0	16.6	9.1	0.0
51R-3, 123-126	784.3	25.7	68.4	14.8	14.8	77.9	0.0	17.1	13.6	0.0
53R-2, 120-122	802.1	0.0	99.2	0.0	0.0	0.0	42.2	54.3	29.6	0.0
53R-6, 47-49	807.4	67.0	93.0	0.0	0.0	17.8	0.0	24.9	38.9	3.2
54R-1, 60-62	809.7	25.8	64.2	0.0	0.0	0.0	0.0	42.6	35.3	2.1
54R-1, 65-67	809.8	22.8	54.5	0.0	0.0	0.0	0.0	41.9	39.3	9.9
54R-1, 125-128	810.4	92.0	39.6	3.9	0.0	0.0	14.8	32.4	19.5	3.3
54R-3, 15-17	812.3	25.2	99.7	0.0	0.0	8.9	0.0	47.1	30.8	0.0
55R-2, 122-124	822.9	71.9	98.3	0.0	0.0	21.6	0.0	50.3	17.5	0.0
56R-1, 70-72	829.1	92.7	25.9	6.8	0.0	100.0	0.0	4.4	0.0	0.0
57R-4, 142-144	844.0	85.8	100.0	5.3	4.1	0.0	0.0	54.4	0.0	6.5
73R-1, 11-13	922.2	100.0	60.1	0.0	23.0	16.9	0.0	7.7	0.0	0.0
73R-5, 46-48	998.6	100.0	43.7	0.0	11.8	0.0	0.0	10.6	0.0	0.0
75R-1, 67-68	1012.0	32.1	29.1	14.0	0.0	0.0	0.0	77.6	0.0	0.0
100R-1, 58-60	1243.6	30.8	22.6	0.0	3.0	100.0	0.0	100.0	0.0	0.0
100R-CC, 20-22	1245.4	100.0	25.0	3.4	6.4	0.0	0.0	7.8	0.0	55.4
101R-1, 22-24	1252.4	100.0	29.7	0.0	6.4	57.4	0.0	7.9	0.0	79.2
101R-2, 12-14	1253.8	100.0	26.2	0.0	2.9	11.1	0.0	19.4	0.0	100.0
101R-2, 92-94	1254.6	100.0	35.1	18.1	7.3	9.3	0.0	12.7	0.0	100.0
101R-3, 41-43	1255.6	100.0	54.9	37.9	0.0	0.0	0.0	58.9	50.4	17.5
101R-4, 2-4	1256.7	100.0	100.0	0.0	0.0	25.0	0.0	0.0	93.1	99.1
102R-2, 30-32	1263.3	100.0	56.4	0.0	0.0	41.1	0.0	49.5	35.2	26.7
102R-3, 40-42	1264.9	100.0	40.9	3.9	0.0	21.2	0.0	13.0	37.5	51.0
102R-3, 118-120	1265.7	100.0	48.8	13.8	0.0	0.0	0.0	17.2	45.3	47.3
103R-3, 39-41	1271.3	100.0	31.5	23.0	10.5	17.5	0.0	85.0	15.5	32.0
103R-3, 45-47	1274.4	63.2	0.0	0.0	0.0	0.0	0.0	0.0	16.8	0.0
103R-3, 98-100	1274.9	100.0	0.0	0.0	0.0	0.0	0.0	0.0	48.8	0.0

Abbreviation of minerals and peaks measured for intensities are as follows. Q: quartz (3.34Å); Feld: feldspar (3.20Å); Ill: illite (9.8Å); Chl: chlorite (7.6Å); Cal: calcite (3.0Å); Ho: hornblende (8.6Å); Clay: clay minerals (15Å); CP: clinoptilolite (9.0Å); Anal: analcite (5.6Å).

Table 2. Analytical data of major-element chemistry of volcanic ash from Site 808.

Sample	mbsf	SiO <sub>2</sub> (wt %)	TiO <sub>2</sub>	Al <sub>2</sub> O <sub>3</sub>	Fe <sub>2</sub> O <sub>3</sub>	MnO	MgO	CaO	K <sub>2</sub> O	Na <sub>2</sub> O	P <sub>2</sub> O <sub>5</sub>	Total	IL*
131-808A-													
1H-3, 71-73 cm	3.7	67.58	0.58	16.16	5.04	0.09	2.16	1.91	2.84	2.75	0.11	99.21	5.11
2H-1, 77-79	7.1	56.53	0.63	15.21	5.30	0.08	3.39	11.54	2.93	1.83	0.24	97.67	13.52
3H-2, 41-43	17.6	63.29	0.76	16.58	7.93	0.53	2.69	1.54	3.21	0.41	0.15	97.09	5.96
131-808B-													
2X-1, 80-82 cm	121.4	62.78	0.75	16.20	7.80	0.52	2.64	1.55	3.18	1.99	0.16	97.56	6.82
9X-4, 92-94	193.6	66.37	0.68	15.54	5.52	0.09	2.17	2.92	2.84	2.00	0.12	98.23	6.12
10X-2, 142-144	200.3	66.20	0.62	13.62	7.39	0.21	2.07	3.46	2.57	2.14	0.18	98.45	7.59
10X-3, 52-54	200.9	66.95	0.72	16.47	4.08	0.11	1.30	2.99	3.80	3.71	0.23	100.35	4.22
11X-1, 115-117	208.0	64.85	0.77	16.96	6.99	0.20	2.63	2.43	2.93	1.74	0.11	99.61	7.06
20X-2, 32-33	289.7	68.91	0.58	14.54	3.97	0.11	1.38	2.59	2.83	3.11	0.14	98.17	4.96
131-808C-													
8R-1, 17-19 cm	366.1	68.80	0.55	15.23	4.93	0.14	1.78	3.17	2.86	2.74	0.25	100.45	6.57
15R-3, 62-63	437.3	56.32	0.66	15.13	11.73	1.16	3.32	4.07	2.84	1.52	1.61	98.36	9.52
15R-4, 33-34	438.5	59.67	0.71	15.87	9.78	0.80	3.06	2.82	3.03	1.82	0.86	98.41	8.54
17R-1, 73-75	453.4	63.68	0.60	13.83	6.80	0.19	1.89	7.39	1.62	2.51	0.46	98.97	10.3
22R-3, 122-124	505.2	73.20	0.28	13.93	2.55	0.06	0.74	1.81	2.55	3.71	0.06	98.88	6.38
27R-6, 32-33	557.1	63.98	0.94	17.61	6.54	0.08	2.06	3.62	1.02	3.56	0.10	99.49	6.97
29R-6, 38-39	575.0	63.29	0.76	16.58	7.93	0.53	2.69	1.54	3.21	3.67	0.15	100.35	7.03
30R-4, 99-100	583.8	69.25	0.50	14.87	4.32	0.11	1.52	2.09	3.00	2.57	0.21	98.44	6.60
30R-5, 119-120	585.5	57.26	0.58	19.25	8.80	0.07	2.91	3.75	0.93	2.62	0.16	96.33	6.98
32R-1, 128-130	598.6	72.61	0.40	14.01	2.38	0.06	0.76	2.00	2.27	3.58	0.09	98.14	6.04
32R-1, 142-144	598.7	74.32	0.33	14.45	2.66	0.07	0.97	1.47	2.37	3.45	0.05	100.12	5.92
32R-1, 147-149	598.8	75.56	0.15	12.75	1.46	0.06	0.36	1.22	2.43	3.96	0.03	97.97	5.83
32R-2, 82-84	599.6	68.61	0.36	16.09	2.43	0.07	1.13	3.72	1.91	3.65	0.11	98.09	5.21
33R-4, 4-6	611.4	62.82	0.52	17.51	9.72	0.05	2.54	2.33	0.95	1.78	0.13	98.34	9.19
34R-4, 126-128	622.3	64.02	0.32	12.42	3.55	0.46	0.98	12.89	1.87	2.85	0.25	99.61	13.29
35R-CC	630	72.04	0.35	13.99	3.65	0.07	1.11	2.03	1.99	2.78	0.05	98.04	
35R-6, 60-62	634.3	72.83	0.32	13.65	3.32	0.07	1.95	2.17	1.94	2.76	0.04	98.05	6.81
37R-1, 30-32	645.8	62.57	0.49	19.77	7.25	0.05	2.87	2.70	0.72	2.92	0.15	99.48	8.31
38R-2, 67-68	657.1	62.10	0.31	20.92	7.59	0.27	2.34	1.93	0.40	2.81	0.04	98.70	6.49
38R-5, 83-85	661.7	63.95	0.75	17.33	5.91	0.09	2.73	1.60	3.33	1.66	0.10	97.45	6.85
38R-6, 69-71	663.1	64.93	0.76	18.08	5.41	0.10	2.55	3.92	1.21	3.36	0.29	100.61	5.89
38R-6, 76-78	663.2	62.31	0.99	17.17	7.71	0.11	3.01	3.49	1.04	3.27	0.19	99.27	6.57
39R-1, 47-49	665.0	62.02	0.28	18.46	9.91	0.06	3.06	1.62	0.40	2.44	0.04	97.79	7.66
39R-3, 31-33	667.8												
39R-3, 52-54	668.0	59.34	0.27	17.50	11.75	0.05	2.61	1.97	0.72	2.69	0.04	96.93	8.16
42R-2, 90-92	695.9	62.60	0.58	18.37	6.81	0.12	2.80	3.74	2.08	1.87	0.10	99.06	7.98
42R-4, 15-17	698.2	62.50	0.26	18.42	8.00	0.07	3.59	1.83	0.59	2.49	0.05	97.81	7.51
43R-2, 115-117	705.9	63.87	0.68	18.29	6.64	0.08	2.66	1.75	2.68	2.05	0.10	98.79	7.62
45R-3, 7-9	725.1	56.08	0.61	23.89	5.10	0.03	3.36	8.22	0.50	1.65	0.10	99.54	3.67
45R-3, 35-37	725.6	61.98	0.49	18.69	7.11	0.05	1.20	6.09	0.60	2.64	0.12	100.95	8.51
45R-3, 61-63	725.6	57.80	0.63	21.01	4.48	0.05	1.17	6.21	0.64	3.72	0.15	96.84	3.76
45R-6, 26-28	729.8	62.57	0.24	19.46	8.54	0.04	1.49	1.44	1.14	2.13	0.05	98.08	8.05
46R-5, 126-129	739.0	66.37	0.28	17.93	5.40	0.06	0.7	2.32	1.01	3.73	0.08	99.24	5.90
46R-5, 135-137	739.1	66.77	0.29	17.93	5.83	0.06	2.44	2.33	0.75	3.62	0.08	100.09	8.30
47R-2, 114-116	743.8	60.63	0.41	19.00	8.19	0.05	2.19	3.69	0.66	2.55	0.08	97.45	5.40
48R-6, 139-140	758.5	64.71	0.66	16.93	5.82	0.60	2.47	2.12	2.84	2.13	0.09	98.37	6.46
50R-5, 2-4	775.6	62.31	0.53	17.11	7.37	0.05	2.35	3.42	2.35	1.94	0.70	98.11	6.76
51R-3, 123-126	784.3	63.87	0.64	16.21	4.80	0.06	2.12	5.42	2.73	1.84	0.11	97.80	8.48
53R-2, 120-122	802.1	62.96	0.48	19.11	5.82	0.06	2.50	4.34	0.64	3.97	0.10	99.98	6.15
53R-6, 47-49	807.4	68.76	0.45	15.96	4.99	0.03	1.50	2.32	1.01	3.20	0.13	98.33	9.47
54R-1, 60-62	809.7	67.04	0.56	16.35	3.55	0.02	1.43	2.96	0.60	3.80	0.16	96.49	8.44
54R-1, 65-67	809.8	61.59	0.58	17.36	7.31	0.05	2.29	2.73	1.49	4.05	0.09	97.52	6.94
54R-1, 125-128	810.4	63.84	0.41	17.26	5.65	0.04	1.96	2.95	0.73	2.78	0.12	95.73	5.52
54R-3, 15-17	812.3	63.48	0.41	17.34	5.62	0.03	2.01	2.95	0.71	3.50	0.12	96.16	7.99
55R-2, 122-124	822.9	55.52	0.87	22.01	9.67	0.03	1.96	5.53	0.96	1.80	0.14	98.49	8.06
56R-1, 70-72	829.1	33.64	0.27	8.78	3.97	2.35	1.51	40.62	1.73	0.67	0.08	93.62	20.58
57R-4, 142-144	844.0	58.10	0.48	20.11	10.96	0.01	2.21	1.78	1.02	1.18	0.06	95.90	9.58
73R-1, 11-13	992.2	64.78	0.73	17.34	6.51	0.14	2.52	0.80	3.47	1.16	0.07	97.51	6.15
73R-5, 46-48	998.6	50.96	0.56	12.98	28.28	0.05	1.78	0.72	2.79	1.11	0.05	99.26	8.67
75R-1, 67-68	1012.0	61.84	0.34	23.35	5.47	0.06	3.65	1.56	0.63	2.12	0.10	99.12	11.92
100R-1, 58-60	1243.6	80.90	0.26	10.77	2.30	0.09	0.99	0.56	1.99	0.75	0.06	98.66	19.19
100R-CC, 20-22	1245.4	80.44	0.25	10.69	2.33	0.10	1.03	0.56	2.06	2.50	0.06	100.01	3.66
101R-1, 22-24	1252.4	75.46	0.25	12.99	2.35	0.80	0.93	0.72	2.65	2.99	0.14	99.27	4.89
101R-2, 12-14	1253.8	72.82	0.20	14.76	1.60	0.05	0.77	0.94	1.55	4.94	0.18	97.81	6.22
101R-2, 92-94	1254.6	74.08	0.25	13.96	1.54	0.06	0.57	0.91	1.13	5.45	0.17	98.12	9.89
101R-3, 41-43	1255.6	72.22	0.34	15.73	2.13	0.07	1.02	3.52	1.09	2.37	0.20	98.68	9.79
101R-4, 2-4	1256.7	72.09	0.41	16.49	0.70	0.05	0.22	2.74	1.64	5.71	0.09	100.14	2.12
102R-2, 30-32	1263.3												
102R-3, 40-42	1264.9	75.71	0.08	13.39	1.09	0.16	0.93	2.63	1.32	3.19	0.03	98.52	6.65
102R-3, 118-120	1265.7	71.69	0.12	15.08	1.37	0.17	1.18	2.21	1.96	3.50	0.04	97.30	6.41
103R-3, 39-41	1271.3	64.56	0.21	21.49	3.68	0.18	3.44	2.51	1.14	2.32	0.09	99.62	13.64
103R-3, 45-47	1274.4	73.07	0.38	14.88	0.82	0.03	0.60	2.79	0.61	4.18	0.05	97.41	9.57
103R-3, 98-100	1274.9	76.73	0.29	13.52	0.47	0.02	0.33	2.38	0.74	3.56	0.07	98.09	5.72

\*IL is ignition loss.

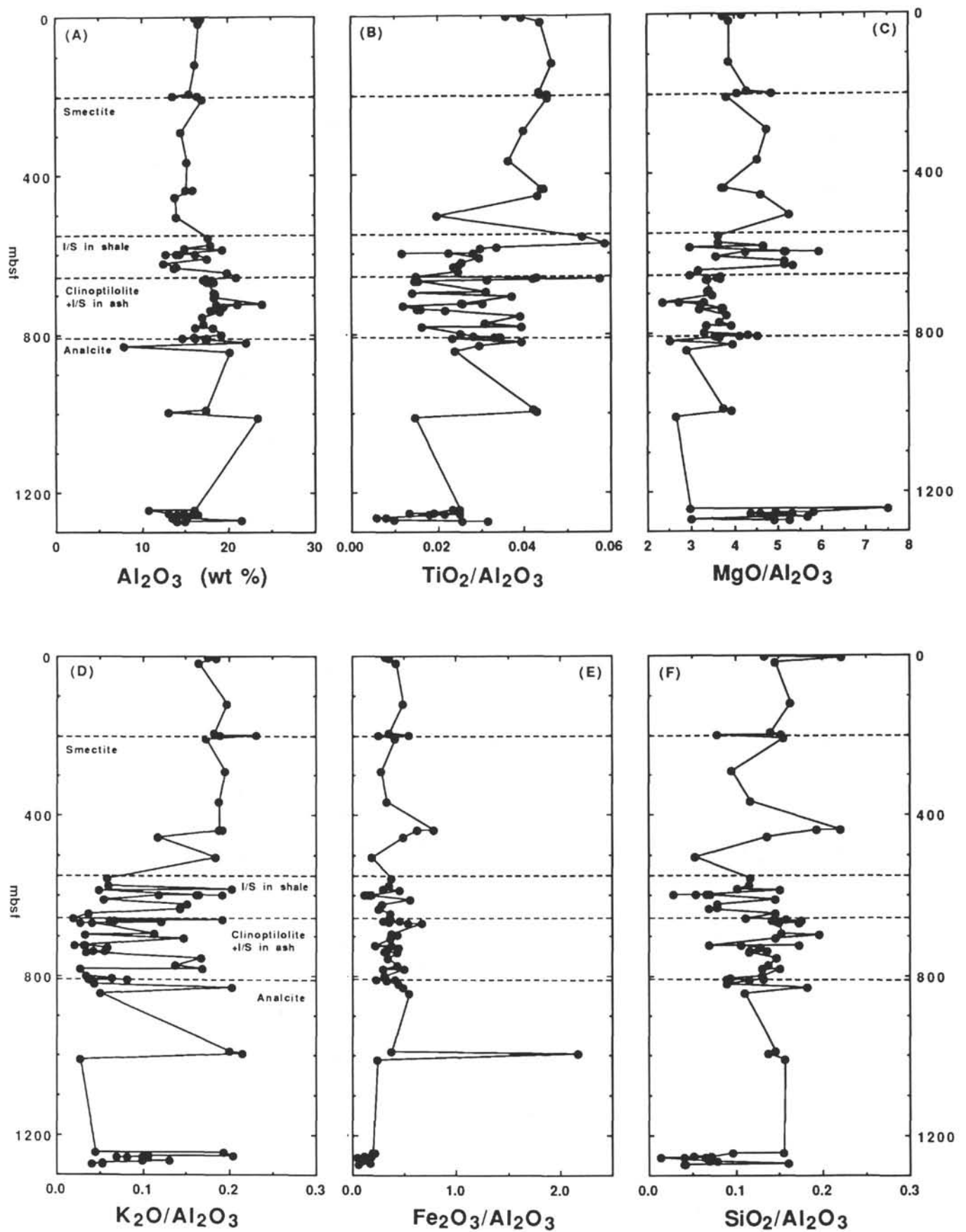


Figure 3. Variation of major chemical constituents of volcanic ash with depth.

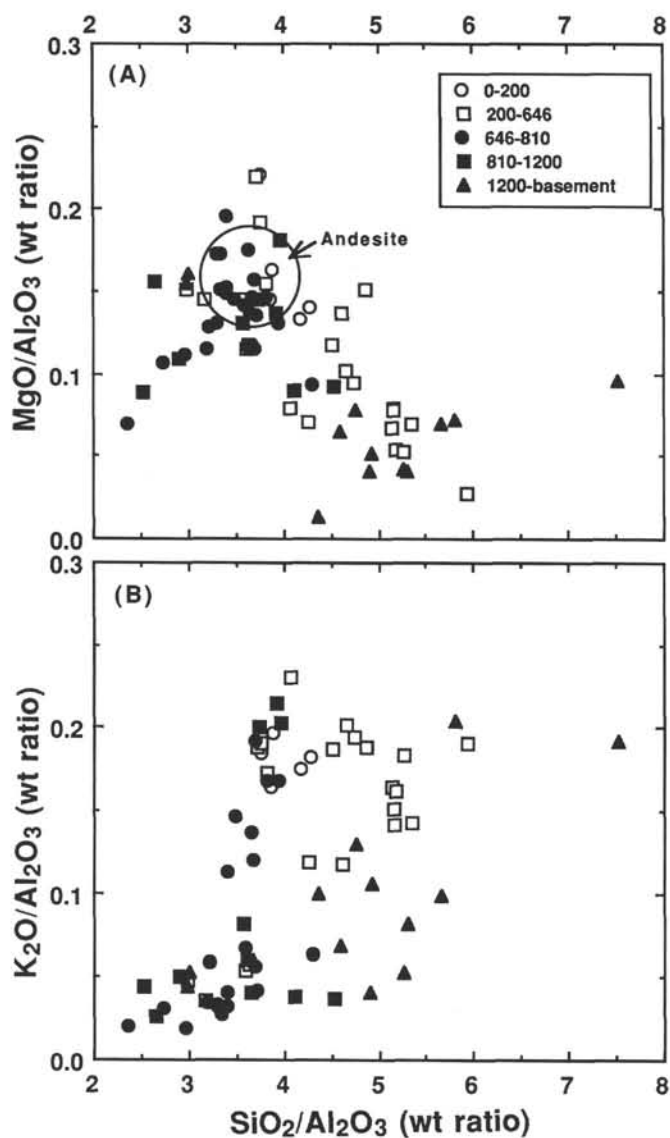


Figure 4. Relation between weight ratios of  $\text{MgO}/\text{Al}_2\text{O}_3$  and  $\text{K}_2\text{O}/\text{Al}_2\text{O}_3$  vs.  $\text{SiO}_2/\text{Al}_2\text{O}_3$ .

mineral assemblages shown in Figure 2B. The plots of  $\text{MgO}/\text{Al}_2\text{O}_3$  vs.  $\text{SiO}_2/\text{Al}_2\text{O}_3$  for samples shallower than 646 mbsf show a negative correlation, although coexisting basic detrital minerals such as chlorite and hornblende obscure this relation. This negative correlation indicates the mixing of andesitic ash and felsic detrital minerals. Below 646 mbsf, the  $\text{SiO}_2/\text{Al}_2\text{O}_3$  and  $\text{MgO}/\text{Al}_2\text{O}_3$  ratios of the same ash are positively correlated, suggesting the possibility that a single process is affecting the  $\text{SiO}_2$  and  $\text{MgO}$  concentrations of ash in the deeper portion.

Above 1200 mbsf, the  $\text{K}_2\text{O}/\text{Al}_2\text{O}_3$  ratio has a less-clear relation to the  $\text{SiO}_2/\text{Al}_2\text{O}_3$  ratio than the case of  $\text{MgO}/\text{Al}_2\text{O}_3$ . The presence of detrital minerals, such as quartz, K-feldspar, K-mica, and hornblende may hide the simple mixing relation observed between  $\text{SiO}_2/\text{Al}_2\text{O}_3$  and  $\text{MgO}/\text{Al}_2\text{O}_3$ . However, the plots of  $\text{K}_2\text{O}/\text{Al}_2\text{O}_3$  vs.  $\text{SiO}_2/\text{Al}_2\text{O}_3$  for samples below 1200 mbsf, where the ash samples are strongly altered, show a weakly positive correlation similar to that between  $\text{MgO}/\text{Al}_2\text{O}_3$  and  $\text{SiO}_2/\text{Al}_2\text{O}_3$ . This means that K behaves in a similar way to Si and Mg in this depth range.

The  $\text{Fe}_2\text{O}_3/\text{Al}_2\text{O}_3$  ratios of all ash samples are positively correlated with the  $\text{MgO}/\text{Al}_2\text{O}_3$  ratios (Fig. 5). The positive correlation is much better in the samples above 810 mbsf, with more scatter in data from

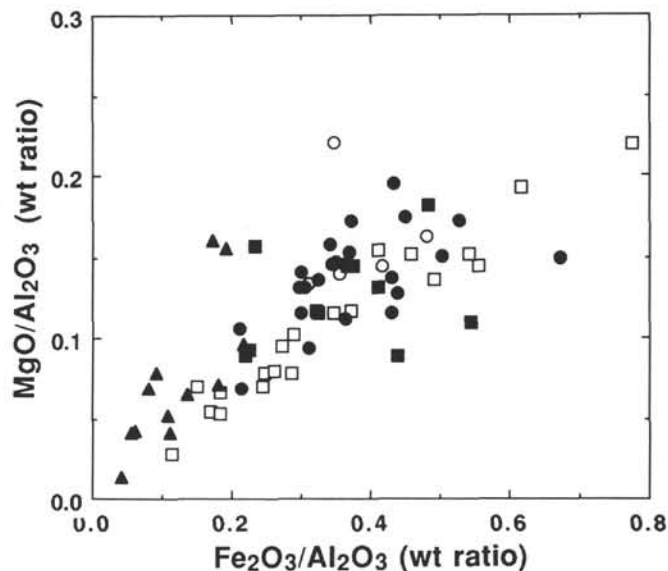


Figure 5. Relation between weight ratios of  $\text{MgO}/\text{Al}_2\text{O}_3$  and  $\text{Fe}_2\text{O}_3/\text{Al}_2\text{O}_3$ . Symbols are the same as those in Figure 4.

deeper samples. Iron is not abundant in interstitial waters, while Mg is one of the major cations there. The data plotting above the general correlation trend in Figure 5 may indicate the incorporation of excess Mg in the solid phase from coexisting interstitial water. An increase of the Mg concentration of the solid phase with depth is consistent with the Mg depletion of coexisting pore fluids (Shipboard Scientific Party, 1991). This indicates that Mg of the pore fluids is fixed in smectite during diagenetic alteration.

#### Interaction Between Ash And Interstitial Water

There appears to be a close relation between the chemical compositions of interstitial water and volcanic ash as a function of depth at Site 808 (Shipboard Scientific Party, 1991). In Figure 6, the  $\text{H}_4\text{SiO}_4$  concentration and K/Cl and Na/Cl ratios of the interstitial waters analyzed during Leg 131 are plotted as a function of depth.  $\text{H}_4\text{SiO}_4$  gradually increases from 500  $\mu\text{M}$  just below the seafloor to 650  $\mu\text{M}$  at 180 mbsf, and then rapidly increases to more than 800  $\mu\text{M}$  between 180 and 200 mbsf. The concentration of  $\text{H}_4\text{SiO}_4$  remains high to a depth of 550 mbsf and then sharply decreases to about 200  $\mu\text{M}$ . The K/Cl ratio of the interstitial waters is characterized by an overall decrease between 0 and 650 mbsf with deflections in this trend near 200 mbsf and 550 mbsf (Fig. 6). The Mg/Cl ratio of the pore waters (not shown in this paper) varies in a similar manner to the K/Cl ratio.

As noted earlier, smectite starts to appear at 200 mbsf and the smectite content drastically increases below 550 mbsf (Fig. 2). Clinoptilolite and analcite first appear in the sediments at 650 and 810 mbsf, respectively. The first occurrence of smectite and the decrease of the K/Cl ratio of the interstitial water in the uppermost 200 mbsf indicate that smectite formation is associated with the removal of K from the interstitial waters. Smectite contains 45 wt%  $\text{SiO}_2$  in its structure, while andesitic glass contains 60 to 65 wt%  $\text{SiO}_2$ . When smectite is formed from andesitic glass,  $\text{SiO}_2$  is released to the interstitial water. This also occurs in the uppermost 200 mbsf at Site 808.

The decrease in the K/Cl ratio of the interstitial waters at 550 mbsf corresponds to the first occurrence of mixed-layered I/S in shales (Underwood et al., this volume). Below 646 mbsf, where clinoptilolite (and maybe I/S) in the ash first appear, the  $\text{H}_4\text{SiO}_4$  concentration and K/Cl ratio of the interstitial waters vary little compared with waters between 550 and 646 mbsf.

As described earlier, the  $\text{SiO}_2/\text{Al}_2\text{O}_3$ ,  $\text{MgO}/\text{Al}_2\text{O}_3$ , and  $\text{K}_2\text{O}/\text{Al}_2\text{O}_3$  ratios of bulk ash layers illustrate the mixing between andesitic glass

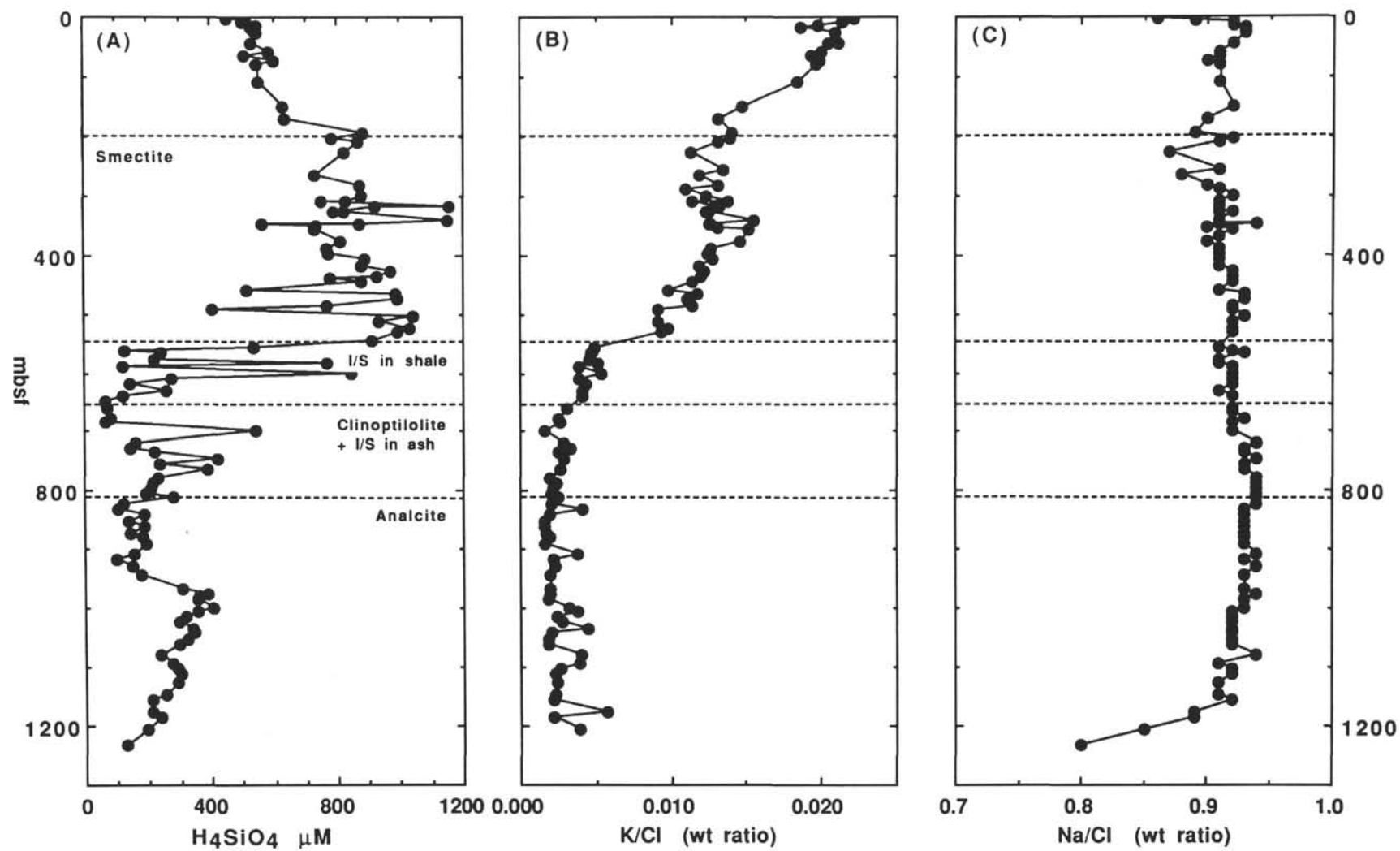


Figure 6. Variation of  $H_4SiO_4$ , K/Cl, and Na/Cl of interstitial waters with depth in relation to alteration mineral assemblages. Analytical data of interstitial water is by Taira, Hill, Firth, et al. (1991).

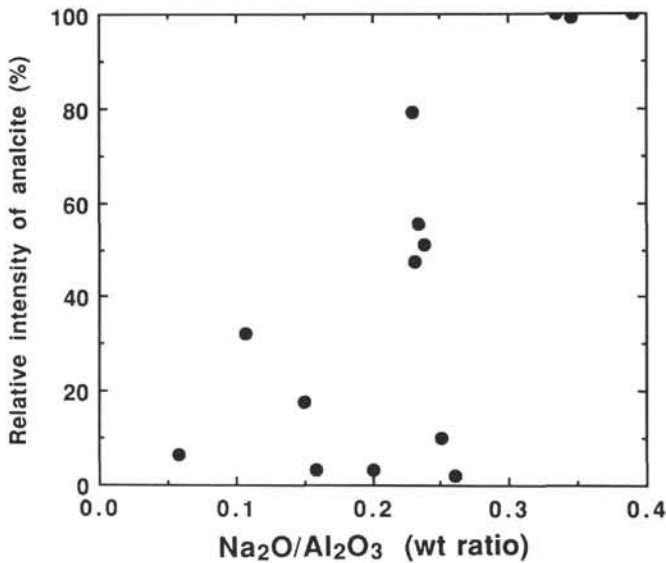


Figure 7. Relation between relative intensities of X-ray diffraction of analcite and  $\text{Na}_2\text{O}/\text{Al}_2\text{O}_3$ .

and detrital minerals in the sediment column above 657 mbsf. By comparing the chemical characteristics of interstitial waters and ash, we suggest that glass decomposition exceeds smectite formation above 646 mbsf. The decrease of the  $\text{H}_4\text{SiO}_4$  concentrations of interstitial waters between 550 and 650 mbsf is probably due to clinoptilolite formation. However, quartz overgrowths precipitating on detrital quartz may occur after illitization of smectites in sedimentary cements (Boles and Franks, 1979). Although an increase of the quartz content of the ash was not observed by X-ray diffractometry in the interval between 550 and 810 mbsf, the precipitation of quartz is also a possible sink for dissolved  $\text{SiO}_2$ .

Analcite is considered to be the major reservoir of Na in this sediment column. The relative intensity of X-ray reflection patterns of analcite tends to increase with the Na content of bulk ash layers (Fig. 7). Because Na is the most abundant cation in interstitial waters, a small variation (in the concentration of dissolved sodium) is hard to detect. In this sediment column, analcite occurs below 810 mbsf. Sodium fixation into analcite is not obvious in the interval between 810 and 1200 mbsf because of the low content of analcite and rare occurrence of ash layers. The decrease of the Na concentration of the interstitial water below 1200 mbsf (Fig. 6C) can be explained by the abundant formation of analcite at these depth (Fig. 2C). Thus, mineral formation by ash alteration also appears to affect the Na content of the interstitial water at the base of this sediment column.

## SUMMARY AND CONCLUSIONS

The mineralogy and major-element chemistry were determined for 72 volcanic ash samples recovered from the sediment column between 4 and 1275 mbsf at ODP Site 808 in the Nankai Trough. The first occurrence depths of crystalline by-products of ash alteration are smectite, 200 mbsf; clinoptilolite, 646 mbsf; and analcite, 810 mbsf. Although I/S formation seems to occur in the sample from 646 mbsf, I/S formation rarely occurs even in the samples from the basement of the column.

In the sediment column above 550 mbsf, glass decomposition occurs faster than mineral formation in terms of component mass balance, but mineral formation becomes more dominant below that depth. During the alteration of ash, Fe is preserved in the solid phase as well as Al and Ti. The concentration of  $\text{H}_4\text{SiO}_4$  in interstitial waters is affected by the initiation of smectite formation at 200 mbsf (increase in  $\text{H}_4\text{SiO}_4$ ) and clinoptilolite formation at 646 mbsf (decrease in  $\text{H}_4\text{SiO}_4$ ). A sharp decrease of the K concentration of the interstitial water is associated with the formation of clinoptilolite (and/or illite).

Clinoptilolite formation probably interferes with the formation of illite in I/S in the sediment column below 646 mbsf. The Mg content of ash layers increases over the same interval, probably as a result of smectite and/or chlorite formation. Analcite forms below 810 mbsf (and particularly below 1240 mbsf), which may cause the observed decrease in the Na concentration of the interstitial water. Thus, the alteration of volcanic ash has a major influence on the chemistry of interstitial waters at Site 808.

## ACKNOWLEDGMENTS

We are indebted to the crew of the *JOIDES Resolution* and the ODP staff. Discussions with M. Kastner and J.M. Gieskes were most helpful. We also thank S.R. Chambers, J.R. O'Neil, and J.W. Hedenquist for their constructive advice on the manuscript. Critical reviews and comments by M.B. Underwood and L.L.S. are gratefully acknowledged. This work was supported by a Grant-in-Aid for Scientific Research on Priority Areas (No. 03248215) from the Ministry of Education, Science and Culture to H.M.

## REFERENCES

- Altaner, S.P., and Grim, R.E., 1990. Mineralogy, chemistry, and diagenesis of tuffs in the Sucker Creek Formation (Miocene), eastern Oregon. *Clays Clay Mineral.*, 38:561-572.
- Anjos, S.M.C., 1986. Absence of clay diagenesis in Cretaceous-Tertiary marine shales, Campos Basin, Brasil. *Clays Clay Mineral.*, 34:424-434.
- Boles, J.R., and Franks, S.G., 1979. Clay diagenesis in Wilcox sandstones of southwest Texas: implication of smectite diagenesis on sandstone cementation. *J. Sediment. Petrol.*, 49:55-70.
- Dunoyer de Segonzac, G., 1970. The transformation of clay minerals during diagenesis and low-grade metamorphism: a review. *Sedimentology*, 15:281-346.
- Gieskes, J.M., and Lawrence, J.R., 1981. Alteration of volcanic matter in deep sea sediments: evidence from the chemical composition of interstitial waters from deep sea drilling cores. *Geochim. Cosmochim. Acta*, 45:1687-1703.
- Gieskes, J.M., Vrolijk, P., and Blanc, G., 1990a. Hydrogeochemistry, ODP Leg 110: an overview. In Moore, J.C., Mascle, A., et al., *Proc. ODP, Sci. Results*, 110: College Station, TX (Ocean Drilling Program), 395-408.
- , 1990b. Hydrogeochemistry of the Northern Barbados accretionary complex transect: Ocean Drilling Project Leg 110. *J. Geophys. Res.*, 95:8809-8818.
- Lawrence, J.R., Drever, J.I., Anderson, T.F., and Brueckner, H.K., 1979. Importance of volcanic alteration in the sediments of site 323: chemistry,  $\text{O}^{18}/\text{O}^{16}$ ,  $\text{Sr}^{87}/\text{Sr}^{86}$ . *Geochim. Cosmochim. Acta*, 43:573-588.
- Machida, H., and Momose, M., 1985. Aso-4: a widespread tephra and its implications to the events of late Pleistocene in and around Japan. *J. Volcanol. Soc. Jpn.*, Ser. 2, 30:49-70. (Japanese with English abstract)
- Matsuhisa, Y., and Matsumoto, R., 1986. Oxygen isotope ratios of interstitial waters from the Nankai Trough and the Japan Trench, Leg 87. In Kagami H., Karig, D.E., and Coulbourn, W.T., et al., *Init. Repts. DSDP*, 87: Washington (U.S. Govt. Printing Office), 853-856.
- Oba, N., Tomita, K., Yamamoto, M., Ohsako, N., and Inoue, K., 1980. Mineral and chemical compositions, and mechanism of formation of volcanic ashes from Sakurajima Volcano, Kyushu, Japan. *J. Jpn. Assoc. Mineral. Petrol. Econ. Geol.*, 75:329-336. (Japanese with English abstract)
- Perry, E., and Hower, J., 1970. Burial diagenesis in Gulf Coast pelitic sediments. *Clays Clay Mineral.*, 18:165-177.
- Sato J., Nakamura, T., Sugawara, S., Takahashi, H., and Sato, K., 1989. Elemental composition of the 1783 eruption products from Asama Volcano. *J. Volcanol. Soc. Jpn.*, Ser. 2, 34:19-39. (Japanese with English abstract)
- Shipboard Scientific Party, 1991. Site 808. In Taira, A., Hill, I.A., Firth, J.V., et al., *Proc. ODP, Init. Repts.*, 131: College Station, TX (Ocean Drilling Program), 71-272.
- Vrolijk, P., 1990. On the mechanical role of smectite in subduction zones. *Geology*, 18:703-707.
- Weaver, C.E., 1958. The effects and geologic significance of potassium "fixation" by expandable clay minerals derived from muscovite, biotite, chlorite, and volcanic material. *Am. Mineral.*, 43:839-861.

Date of initial receipt: 1 October 1991

Date of acceptance: 23 April 1992

Ms 131SR-118